blood®
Regular Article

THROMBOSIS AND HEMOSTASIS

Type 2B von Willebrand disease mutations differentially perturb autoinhibition of the A1 domain

Emily R. Legan,[1] Yi Liu,[2,3] Nicholas A. Arce,[1] Ernest T. Parker,[1] Pete Lollar,[1] X. Frank Zhang,[3] and Renhao Li[1]

[1]Aflac Cancer and Blood Disorders Center, Children's Healthcare of Atlanta, Department of Pediatrics, Emory University School of Medicine, Emory University, Atlanta, GA; [2]Department of Bioengineering, Lehigh University, Bethlehem, PA; and [3]Department of Biomedical Engineering, University of Massachusetts Amherst, Amherst, MA

KEY POINTS

- All represented type 2B VWD mutations share regions of enhanced dynamics and reduced mechanical stability.
- Heterogeneity displayed by reported type 2B VWD mutants is detected in single-domain monomeric fragments.

Type 2B von Willebrand disease (VWD) is an inherited bleeding disorder in which a subset of point mutations in the von Willebrand factor (VWF) A1 domain and recently identified autoinhibitory module (AIM) cause spontaneous binding to glycoprotein Ibα (GPIbα) on the platelet surface. All reported type 2B VWD mutations share this enhanced binding; however, type 2B VWD manifests as variable bleeding complications and platelet levels in patients, depending on the underlying mutation. Understanding how these mutations localizing to a similar region can result in such disparate patient outcomes is essential for detailing our understanding of VWF regulatory and activation mechanisms. In this study, we produced recombinant glycosylated AIM-A1 fragments bearing type 2B VWD mutations and examined how each mutation affects the A1 domain's thermodynamic stability, conformational dynamics, and biomechanical regulation of the AIM. We found that the A1 domain with mutations associated with severe bleeding occupy a higher affinity state correlating with enhanced flexibility in the secondary GPIbα-binding sites. Conversely, mutation P1266L, associated with normal platelet levels, has similar proportions of high-affinity molecules to wild-type (WT) but shares regions of solvent accessibility with both WT and other type 2B VWD mutations. V1316M exhibited exceptional instability and solvent exposure compared with all variants. Lastly, examination of the mechanical stability of each variant revealed variable AIM unfolding. Together, these studies illustrate that the heterogeneity among type 2B VWD mutations is evident in AIM-A1 fragments.

Introduction

von Willebrand factor (VWF) circulates in the plasma as a large, concatenated glycoprotein and facilitates primary hemostasis through its multiple domains.[1,2] Many VWF functions and regulatory mechanisms are governed by shear forces in the bloodstream. When subendothelial collagen tethers VWF to the wounded vessel, tensile forces stretch the VWF multimer to expose individual monomers. Elevated forces applied to the A1 domain induce local conformational changes before glycoprotein Ibα (GPIbα) binds.[3] A1 binding to GPIbα is partly regulated by the terminal residues flanking the A1 disulfide (Cys1272-Cys1458), a region we have named the VWF autoinhibitory module (AIM) (Figure 1). Studies on various truncated AIM-A1 fragments indicate that AIM preservation correlates inversely with the binding affinity of A1 and GPIbα,[4-6] with longer, more intact AIM exhibiting lower A1 affinity. Full inhibitory function necessitates adequate stability of both the N- and C-terminal AIMs (Figure 1B), which can be compromised by excessive shear, activators such as antibiotic ristocetin or antibody 6G1,[5] or desialylation or removal of O-glycans decorating the AIM,[6,7] collectively providing strong evidence that these discontinuous residues form a cooperative functional unit.

Missense mutations in the A1 domain underlying type 2B von Willebrand disease (VWD) have long epitomized active VWF regardless of shear. Type 2B VWD mutations are classified by enhanced binding to GPIbα and increased sensitivity to ristocetin activation. Clinical reports indicate that whereas type 2B mutations share these features, other properties present more heterogeneously depending on the causative mutation.[8] For instance, many patients with type 2B VWD experience reduced platelet counts upon stimuli such as infection or pregnancy;[9,10] however, patients with mutation P1266L typically have normal platelet concentrations,[11] whereas mutation V1316M induces severe, chronic thrombocytopenia[12] (supplemental Table 1, available on the *Blood* website). Furthermore, patients with P1266L have multimer distributions akin to normal plasma,[11,13,14] whereas other mutations variably reduce high-molecular weight multimers (HMWMs), with V1316M having the greatest reduction.[8]

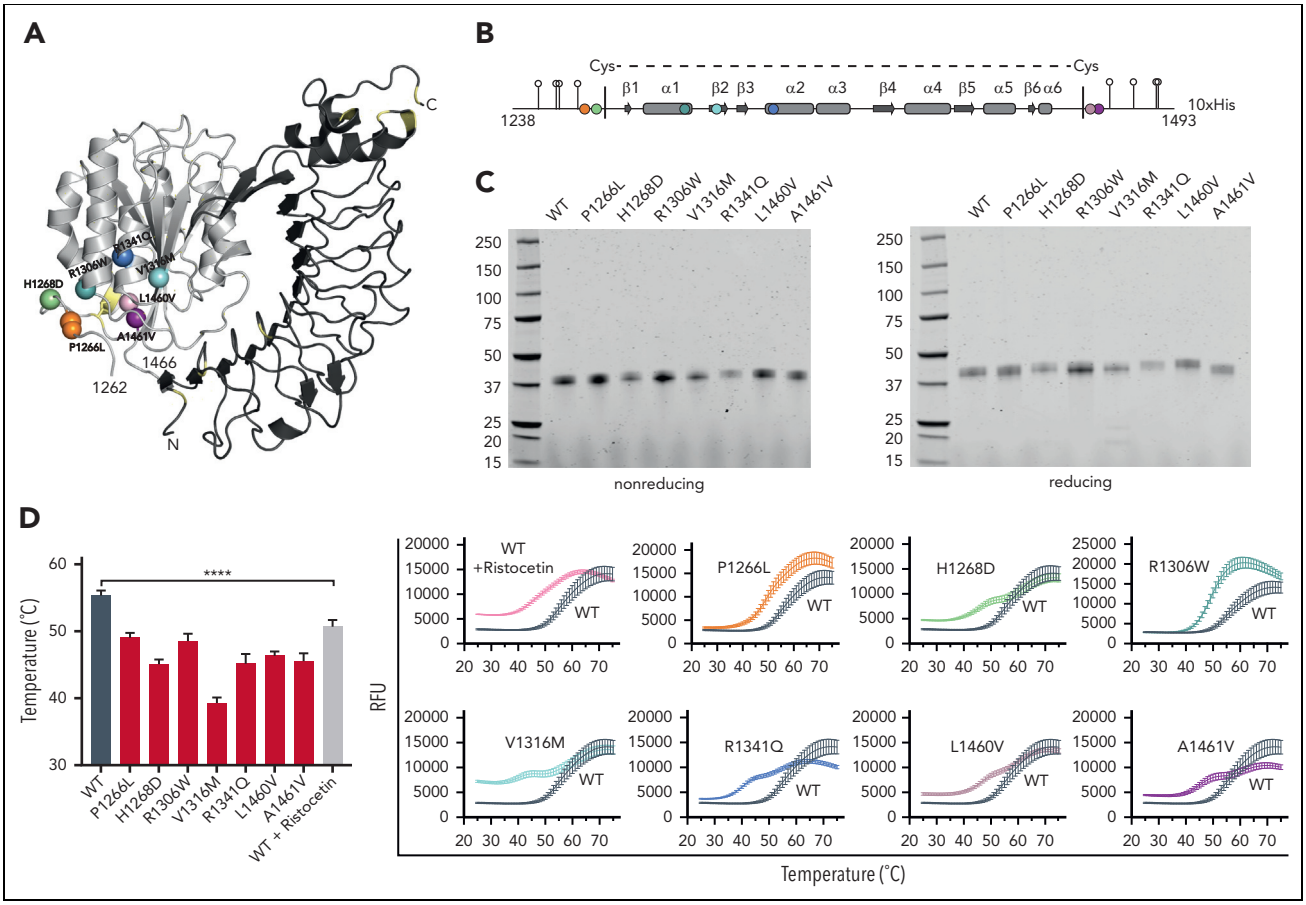

Figure 1. Type 2B mutations destabilize purified AIM-A1. Locations of represented type 2B mutations on the 3-dimensional crystal structure (PDB:7A6O aligned with PDB:1SQ0 GPIb chain) (A) and linearized schematic on AIM-A1 (B). (C) Coomassie-stained sodium dodecyl sulfate– polyacrylamide gel electrophoresis gels of purified AIM-A1 variants under nonreducing (left) and reducing (right) conditions. (D) Unfolding temperatures (Tm_{50}) of AIM-A1 variants as determined by the first derivative of thermal shift data (n = 4 independent replicates). Significance was determined via 1-way analysis of variance with post hoc Tukey test correction compared with WT, where ****P < .0001.

Initially, all reported type 2B mutations localized near the bottom of the disulfide-delimited A1 domain; however, identification of mutation H1268D was the first of several later identified type 2B mutations located in the AIM.[15,16] Identification of naturally occurring mutations in this region further suggests that AIM stability is an essential facet of VWF function. Unlike other types of VWD, which have mutations distributed across several domains, type 2B mutations are restricted to AIM or A1.[2] Consistently, recombinant AIM-A1 proteins (VWF residues Gln1238-Asp1493) have been shown to recapitulate the activity of full-length VWF and its response to various activating factors.[5] With recent findings regarding AIM function, it becomes plausible that the gain-of-function phenotype observed in type 2B VWD imparts loss of inhibitory function. Furthermore, we postulated whether variable loss of autoinhibition could explain heterogenous platelet counts and bleeding severity in patients with type 2B VWD. To investigate how A1 autoinhibition is maintained in type 2B VWD, we generated 7 recombinant AIM-A1 proteins bearing type 2B mutations (Figure 1A-C) and comparatively examined the mutational effect on AIM-A1 thermodynamics, binding kinetics, and mechanical stability. We report evidence of heterogeneity displayed by type 2B variants at the single-domain level on all examined parameters, providing insights into allosteric mechanisms by which A1 activation may occur.

Methods

Materials

Recombinant human GPIbα ligand-binding domain (LBD) proteins were expressed and purified as described previously.[5,6] DNA primers were supplied by Integrated DNA Technologies (Coralville, IA); cell culture dishes and flasks were from Corning (Corning, NY); ristocetin was purchased from MP Biomedicals (Santa Ana, CA); bovine serum albumin and guanidine hydrochloride were from Millipore-Sigma (Burlington, MA); and Tris (2-carboxyethyl) phosphine hydrochloride was from GoldBio (St. Louis, MO).

Recombinant protein expression

Recombinant VWF AIM-A1 proteins (residues 1238-1493) with a C-terminal decahistidine tag were expressed in stably transfected baby hamster kidney cells. BioSpy-AIM-A1 and type 2B mutants (residues 1238-1493) appended with an N-terminal BioTag (LNDIFEAQKIEWH) and C-terminal decahistidine tag and SpyTag (AHIVMVDAYKPTK) were transiently expressed in Expi293F cells using a TransIT-PRO transfection reagent kit (Mirus Bio LLC, Madison, WI).[5] Details on DNA primers for site-directed mutagenesis and purification are provided in the supplemental Material.

Thermal shift assay

AIM-A1 proteins were diluted to 5 μM and mixed with SYPRO Orange protein stain (1:1000 [volume to volume ratio (%)]) (Thermo Fisher Scientific) in phosphate-buffered saline. Thermal denaturation was measured in a real-time polymerase chain reaction instrument with exported curves fit to a Boltzmann sigmoidal function. Apparent melting temperatures were obtained by plotting the first derivative of the fluorescence emission as a function of temperature (−dF/dT).

Analytical ultracentrifugation

Sedimentation velocity experiments were performed at 20°C in a Beckman Coulter XLI analytical ultracentrifuge as previously described.[6]

Biolayer interferometry

Binding experiments were performed on an Octet QK^e instrument as previously described[5] with details in the supplemental Material.

Hydrogen-deuterium exchange (HDX) mass spectrometry

Experiments were largely performed as described[6] with detailed information in the supplemental Material.

Single-molecule force measurements

A dual-beam mini-tweezers instrument was used to perform the AIM unfolding experiments to characterize the AIM-A1 variants at the single-molecule level. The experiments were performed under 5 different pulling speeds (50 nm/s, 100 nm/s, 200 nm/s, 400 nm/s, and 500 nm/s) in Tris-buffered saline (10 mM Tris and 150 mM sodium chloride, pH 7.5) at room temperature. Purified biotinylated recombinant BioSpy-AIM-A1 and mutants were attached to 2.0-μm streptavidin-coated beads and then brought to interact with 2.0-μm streptavidin-coated beads conjugated with SpyCatcher-DNA handles. Upon AIM unfolding, unfolding extension is defined as the increase in end-to-end distance between the point of unfolding and the point at which the force at unfolding is reestablished. To find the most probable extension at various forces, the force-extension data were first binned by force and the extensions were then plotted in a histogram. The most probable extensions were determined by conducting a Gaussian fit to the histograms. The force-extension data were fitted to the worm-like chain model.[17] Unfolding was also analyzed according to the Bell-Evans model to determine the most probable unfolding force of the protein at different loading rates.[18-20]

Results

AIM-A1 stability is reduced by type 2B mutations

Of the 7 type 2B variants studied in this study (Figure 1A-C), mutations in the N-terminal AIM (P1266L and H1268D), the A1 domain (R1306W, V1316M, and R1341Q), and the C-terminal AIM (L1460V and A1461V) were represented. Their thermodynamic stability was assessed via thermal denaturation (Figure 1D). Wild-type (WT) underwent thermal denaturation at 55.6°C ± 0.5°C, whereas type 2B mutants denatured at temperatures at least 5°C lower, indicating that type 2B mutations reduce the global stability of AIM-A1. Of the examined mutants, P1266L had the highest thermal inflection point at 50.6°C ± 0.9°C, close to that of WT treated with 0.5 mg/mL ristocetin (50.9°C ± 0.8°C). Although no determined structure of the A1 domain has shown direct contacts between the A1 domain and Pro1266 nor the proline-rich segment to which ristocetin binds,[21] this observation implicates these proline residues of the AIM as important for overall A1 stability. V1316M had the lowest thermal inflection point at 39.5°C ± 0.6°C, demonstrating that this mutation associated with persistent thrombocytopenia has the greatest reduction in stability. All other variants, expectedly, had thermal inflection points between those of P1266L and V1316M, consistent with the variable platelet concentrations observed in patients. In addition, all type 2B mutants (except for R1306W) and WT treated with ristocetin displayed 2 inflection points or slopes in their denaturation curves, potentially indicating disruption to the native folding pathway. Substitution to a very large, hydrophobic residue may limit possible unfolding pathways to explain this exception observed for R1306W. Despite their reduced stability, the mutants were monomeric (supplemental Figure 1), consistent with desialylated or other destabilized truncated AIM-A1 fragments.[4,6,22]

Some, but not all, type 2B variants have greater proportions of high-affinity molecules

Using biolayer interferometry, we confirmed that the type 2B variants exhibited enhanced binding to the GPIbα LBD. WT had no detectable interaction with immobilized recombinant GPIbα LBD, whereas all type 2B variants bound with a measured affinity in the micromolar range (supplemental Figure 2; supplemental Table 3). To capture enhanced resolution of VWF-GPIbα binding behavior, we measured binding between AIM-A1 variants and recombinant LBD bearing the platelet-type VWD W230L mutation (PT-LBD).[23,24] Sensorgram data with the PT-LBD showed increased response magnitude of all variants and clarified the 2:1 global fit of the data (Figure 2). Although stoichiometrically, 1 AIM-A1 molecule binds 1 LBD, the 2:1 fit more accurately described AIM-A1 dissociation (supplemental Figure 3), consistent with 2 distinct off-rates characterizing the A1-LBD flexbond.[25] The low-affinity AIM-A1 state had a measured dissociation equilibrium constant (K_d) in the hundreds-of-nanomolar range, averaging 360 ± 38 nM, whereas the high-affinity state K_d was in the tens-of-nanomolar range averaging to 41 ± 3 nM (Figure 2; Table 1). Both low- and high-affinity states had similar association rate constants (k_a), with k_a of all variants averaging $3.3 \times 10^5 \pm 0.3 \times 10^5$ $M^{-1}s^{-1}$ and $2.2 \times 10^5 \pm 3 \times 10^5$ $M^{-1}s^{-1}$, respectively. The measured affinities differed by their dissociation rate constants (k_d), with low-affinity k_d averaging $107 \times 10^{-3} \pm 4 \times 10^{-3}$ s^{-1}, whereas the high-affinity k_d was ~10 times slower, averaging $8 \times 10^{-3} \pm 0.3 \times 10^{-3}$ s^{-1} for all variants.

Biphasic fittings of the data produced estimates of the relative abundance of the low- and high-affinity states. Both WT and P1266L had proportions of high-affinity molecules at 21% ± 13% and 27% ± 6%, respectively. Other mutants had a greater relative abundance of high-affinity molecules ranging from 32.3% ± 4% (R1341Q) to 43.6% ± 5% (V1316M).

Type 2B mutations alter the conformational dynamics of the A1 domain

Previous studies have sought the structure of a high-affinity A1 domain by crystallizing variants with type 2B mutations; however, the determined structures resembled WT with minimal

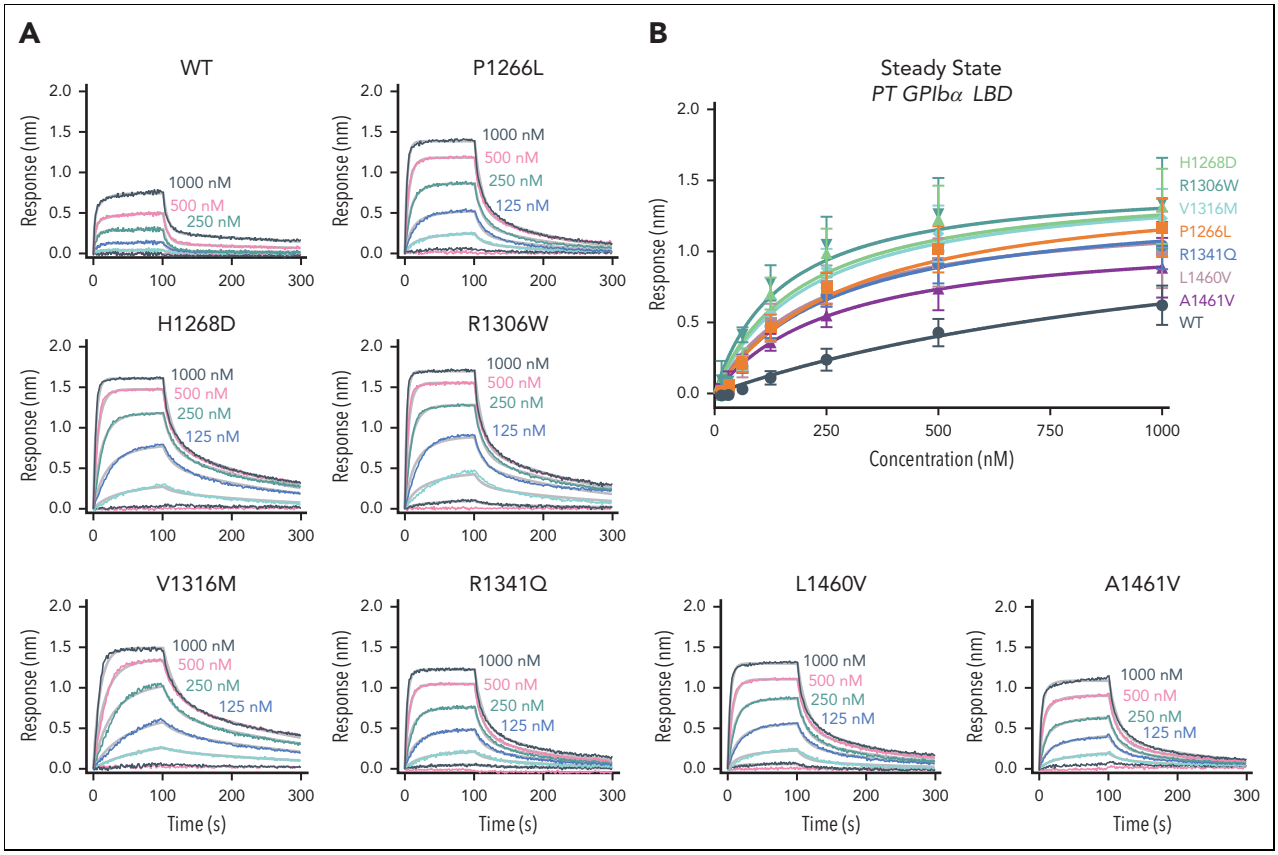

Figure 2. Fast- and slow-dissociating AIM-A1 molecules describe a 2-state binding model to GPIbα. (A) Representative sensorgrams of indicated AIM-A1 variants at concentrations from 1 μM to 15.625 nM show that type 2B VWD mutants yield greater binding response to immobilized PT-LBD (W230L). (B) Steady-state binding data of sensorgrams displaying means ± standard deviations of n = 3 independent replicates.

differences.[26,27] To uncover structural differences that distinguish the lower affinity and hyperactive AIM-A1 conformations, we performed HDX to inspect AIM-A1 dynamics in solution at pD 7.0 and 20°C. A distinct advantage of HDX is that the observed exchange pattern represents the total conformational landscape of protein molecules as opposed to biasing conformations amenable to crystallization.[28,29]

Heatmaps displaying the relative deuterium uptake of the type 2B variants revealed differential exchange patterns (Figure 3;

Table 1. Kinetic data parameters describing binding of AIM-A1 variants to platelet-type GPIbα LBD

	Low-affinity AIM-A1				High-affinity AIM-A1			
	K_D (nM)	$k_a \times 10^5$ ($M^{-1}s^{-1}$)	$k_d \times 10^{-3}$ (s^{-1})	Percent abundance	K_D (nM)	$k_a \times 10^5$ ($M^{-1}s^{-1}$)	$k_d \times 10^{-3}$ (s^{-1})	Percent abundance
WT	503 ± 56.6	3.97 ± 0.37	195 ± 6.5	79.0 ± 12.7	30.2 ± 3.92	1.33 ± 0.24	3.39 ± 0.26	21.0 ± 12.7
P1266L	317 ± 22.2	3.70 ± 0.23	113 ± 3.16	73.0 ± 6.0	34.1 ± 2.45	2.66 ± 0.20	8.34 ± 0.23	27.0 ± 6.0
H1268D	312 ± 29.7	3.13 ± 0.25	86.9 ± 3.0	57.33 ± 1.2	26.9 ± 1.46	2.29 ± 0.11	6.18 ± 0.14	42.66 ± 1.2
R1306W	197 ± 16.0	5.07 ± 0.39	90.3 ± 2.9	61.33 ± 3.2	18.5 ± 1.20	3.49 ± 0.21	6.16 ± 0.16	38.66 ± 3.2
V1316M	635 ± 91.1	1.10 ± 0.12	58.1 ± 2.5	56.33 ± 4.7	44.9 ± 2.51	1.11 ± 0.49	4.97 ± 0.14	43.6 ± 4.7
R1341Q	319 ± 25.1	3.28 ± 0.22	98.7 ± 2.4	67.7 ± 4.0	41.3 ± 2.97	2.35 ± 0.18	7.20 ± 0.22	32.3 ± 4.0
L1460V	311 ± 35.9	2.40 ± 0.22	102 ± 1.9	60.7 ± 9.2	39.3 ± 4.27	3.22 ± 0.55	12.3 ± 0.66	43.5 ± 9.2
A1461V	283 ± 26.2	3.82 ± 0.27	111 ± 7.3	62.0 ± 8.5	96.1 ± 6.74	1.51 ± 0.24	16.0 ± 0.67	38.0 ± 8.5
Average	360 ± 37.9	3.31 ± 0.26	107 ± 3.8	63.7 ± 6.2	41.4 ± 3.19	2.24 ± 0.28	8.07 ± 0.31	35.8 ± 6.2

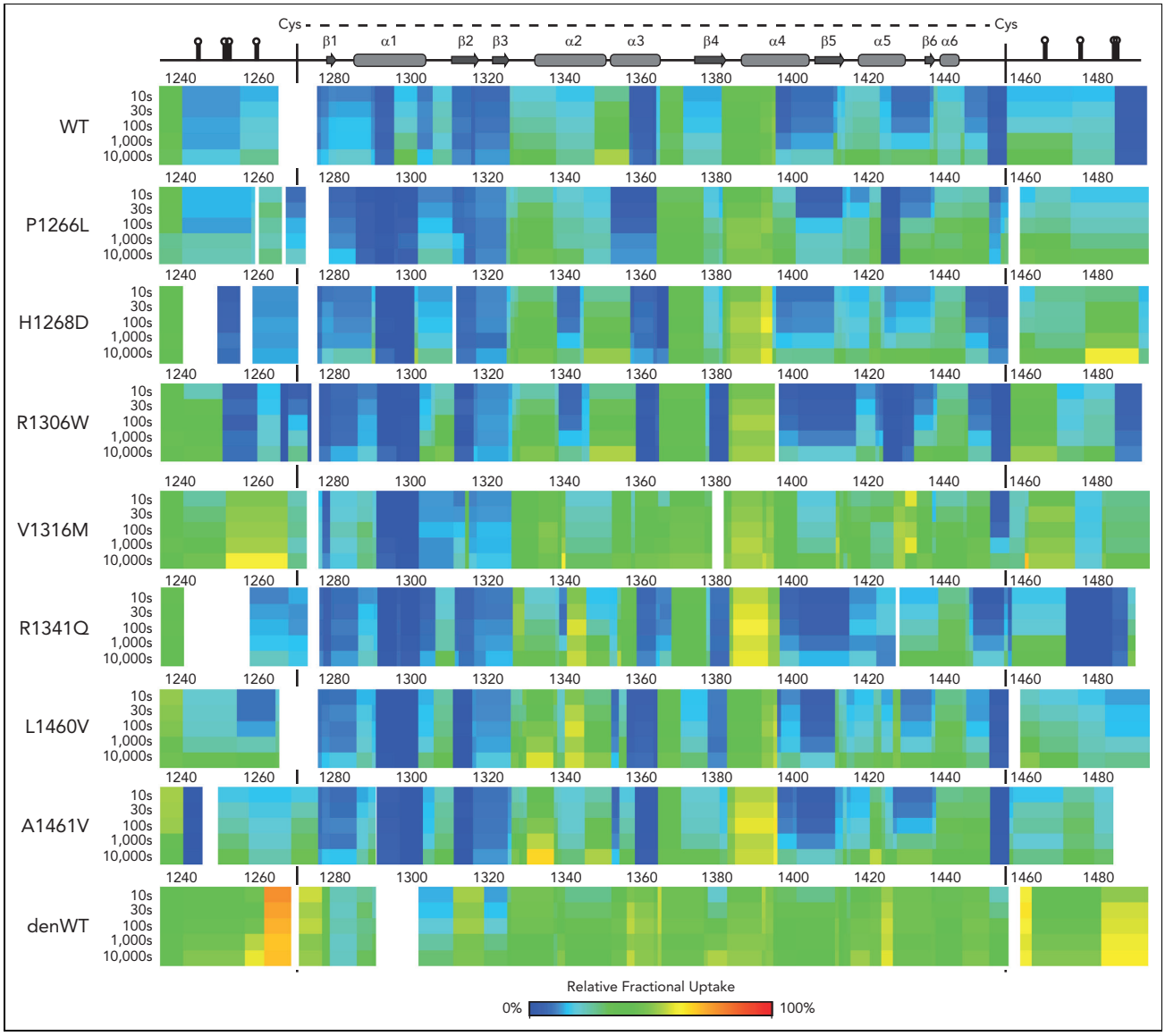

Figure 3. HDX data show differences in protection among AIM-A1 variants. Heatmaps of relative deuterium uptake produced in DynamX at indicated time points between 10 and 10 000 seconds. The color spectrum represents fractional deuterium uptake at near-residual resolution by subtracting exchange differences of overlapping peptides. A linear schematic of secondary structure is aligned to heatmaps and displayed above. WT AIM-A1 was denatured as described in "Materials" before HDX to compare maximal exchange. Values are produced from n = 3 technical replicates.

supplemental Figures 4 and 5). The rate and extent of HDX was much greater in V1316M compared with the other variants, suggesting that the mutant protein adopts little stable fold; however, residues in the α1 helix and central β1 strand retained protection unobserved in denatured WT, indicating that V1316M maintains a folding core.[30] Interestingly, V1316M underwent different exchange patterning across the α2-α3 helices, the same interface mediating GPIbα binding, indicating multiple conformations of this interface that is not observed in WT nor the other represented mutants (supplemental Figure 6). This atypical HDX patterning in conjunction with the observation that low-affinity V1316M molecules dissociate from PT-LBD ~2 times more slowly than all other low-affinity populations of AIM-A1 suggests that V1316M is anomalous from other type 2B variants.

Type 2B mutations enhance the exposure of secondary GPIbα-binding sites

To quantify observed HDX differences, we comparatively analyzed the magnitude and statistical relevance of the relative deuterium uptake of common peptides between mutant and WT proteins in the fastest exchange time tested (Figure 4). At 10 seconds, all type 2B mutants showed significant deuterium uptake compared with WT in the α3β4 loop (Figure 4H), a site involved in electrostatic contacts to leucine-rich repeat 4 (LRR4) and LLR5 in the GPIbα LBD.[27] Furthermore, among the type 2B mutants, there are variable rates of HDX in the β3α2 loop (Figure 4I; supplemental Figure 7), the region proximal to the β3 strand where A1 forms an extended β-sheet complex with the β-switch of the LBD[26,31] (Figure 1A). The variant with fastest exchange in this region was, unsurprisingly, V1316M; however,

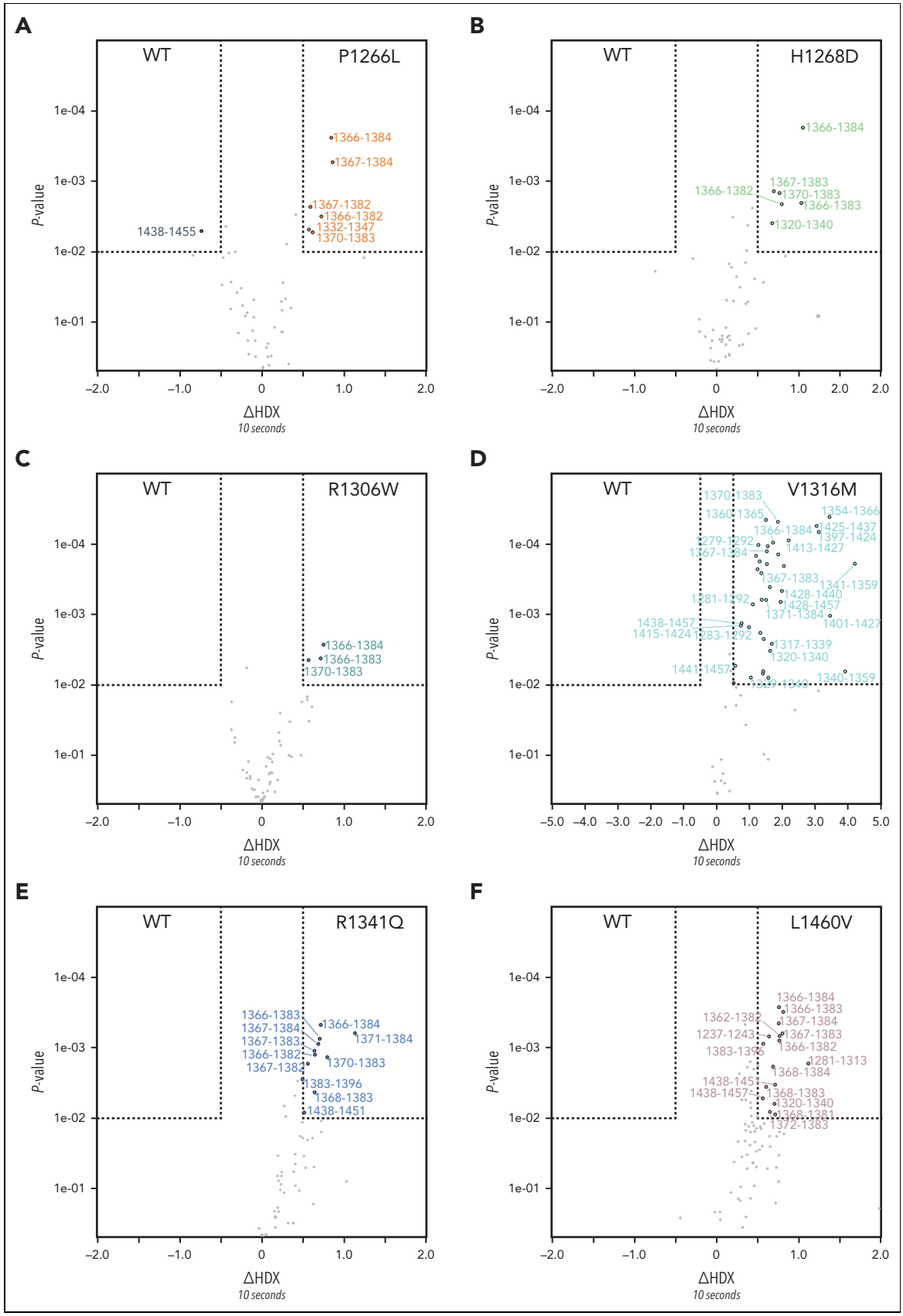

Figure 4. AIM-A1 and type 2B mutants reveals conformational differences. (A-G) Volcano plots showing differences in deuterium uptake among shared peptides after 10 seconds of exchange. The threshold for significance (data points above the dotted lines) requires both statistical significance of $P \leq .01$ and a minimum difference of 0.5 dalton per peptide. Plots were generated using HD-eXplosion version 1.2. Peptides with significant HDX differences are displayed in color in the quadrant of the

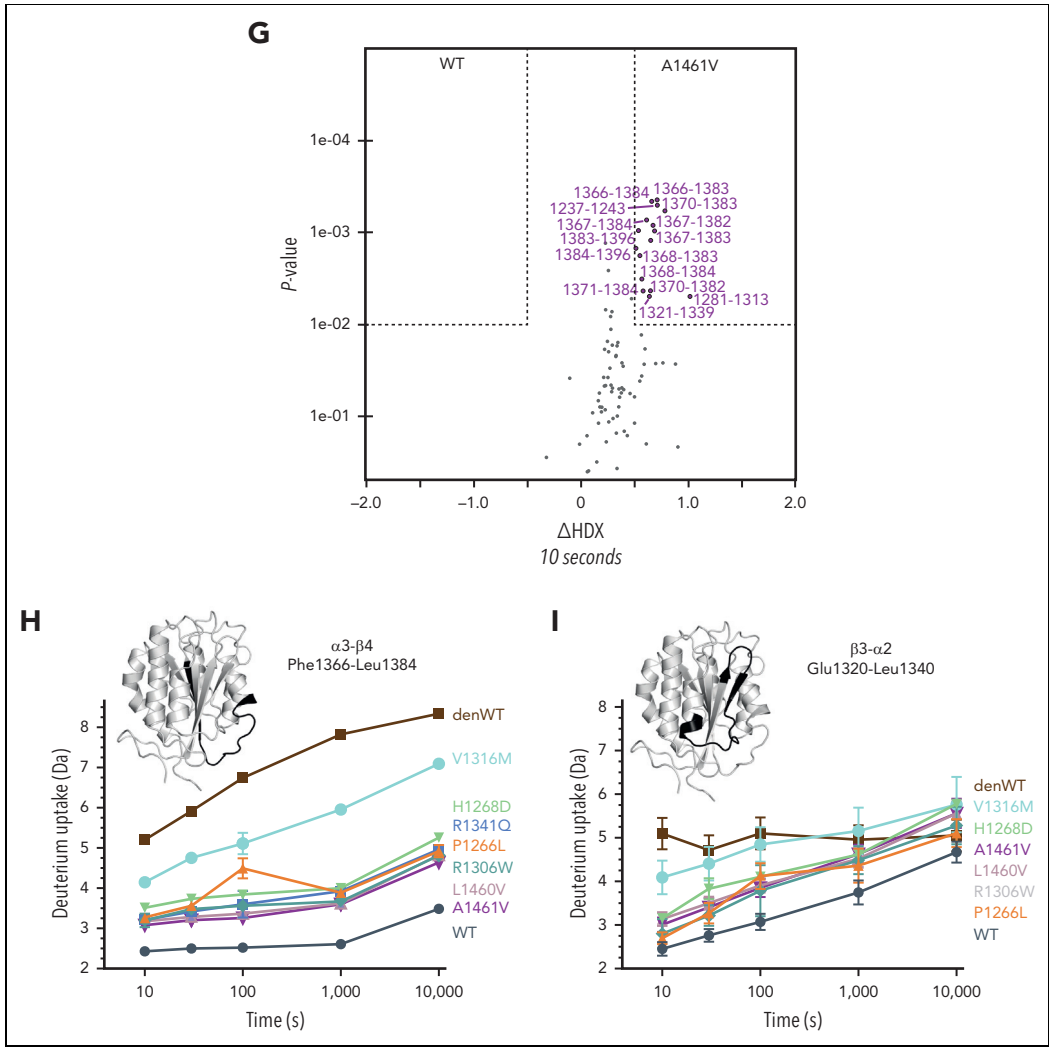

Figure 4 (continued) AIM-A1 variant with greater deuterium uptake. (H) Relative deuterium uptake over time for a representative peptide in the α3β4 loop. All type 2B VWD mutations tested have increased solvent accessibility in this region compared with WT. (I) Representative uptake of peptide in β3α2 loop showing P1266L has protection comparable with WT in this region at the fastest time point tested but loses this protection over time similarly to other type 2B VWD mutants. The crystal structure of AIM-A1 (PDB:7A6O) in gray and the indicated peptide mapped in black are displayed on each graph.

all variants underwent significantly more exchange than WT at 100 seconds. Greater deuterium uptake in type 2B mutants in these regions indicates higher flexibility and increased solvent accessibility, thereby, providing a plausible molecular basis by which these mutants confer spontaneous binding to GPIbα. The extent of deuterium uptake was greater in the α3β4 loop in all mutants at all time points tested, with V1316M incorporating the most deuterium. At the fastest time point tested, P1266L and WT exhibited similar dynamics in the β3α2 loop, suggesting protection of this region is partially preserved in P1266L. Unlike WT AIM-A1 and its mutant counterparts, the conformational dynamics of AIM-A1 in the recombinant protein was highly similar to that in purified plasma-derived VWF, with similar HDX rates and relative deuterium uptake in representative peptides in the α3β4 and β3α2 loops (supplemental Figure 8).

Type 2B mutations reduce mechanical force resistance of the AIM

We recently found that the mechanical stability of the AIM could be disrupted with type 2B mutations H1268D or R1341Q as well as treatment with the ristocetin-mimetic antibody 6G1.[5] Residues His1268 and Arg1341 contact Glu1305 and Glu1264, respectively, when cocrystallized with stabilizing nanobody VHH81,[5] demonstrating direct binding between the AIM and A1 in addition to the salt-bridge proposed between Asp1261 and A1 residues.[32] Naturally, we hypothesized that other type 2B mutations would induce a similar effect. We used single-molecule force spectroscopy with AIM-A1 variants containing a biotinylated tag and a SpyTag (BioSpy-AIM-A1) for iterative pulling and retraction cycles of the N and C termini of AIM-A1 (Figure 5A). Consistent with our previous observations, a small, singular unfolding event occurred, albeit at lower forces, indicating that these type 2B mutations reduce the force threshold necessary to relieve autoinhibition while sustaining AIM cooperativity.

We found that all type 2B mutations except R1306W reduced the contour length (L_c) of the AIM (Figure 5B; Table 2), indicating that the cohesive bond network maintaining AIM cooperativity and A1 protection is disrupted before the application of mechanical force. Although R1306W did not affect the contour length of the AIM, the persistence length (L_p) was reduced

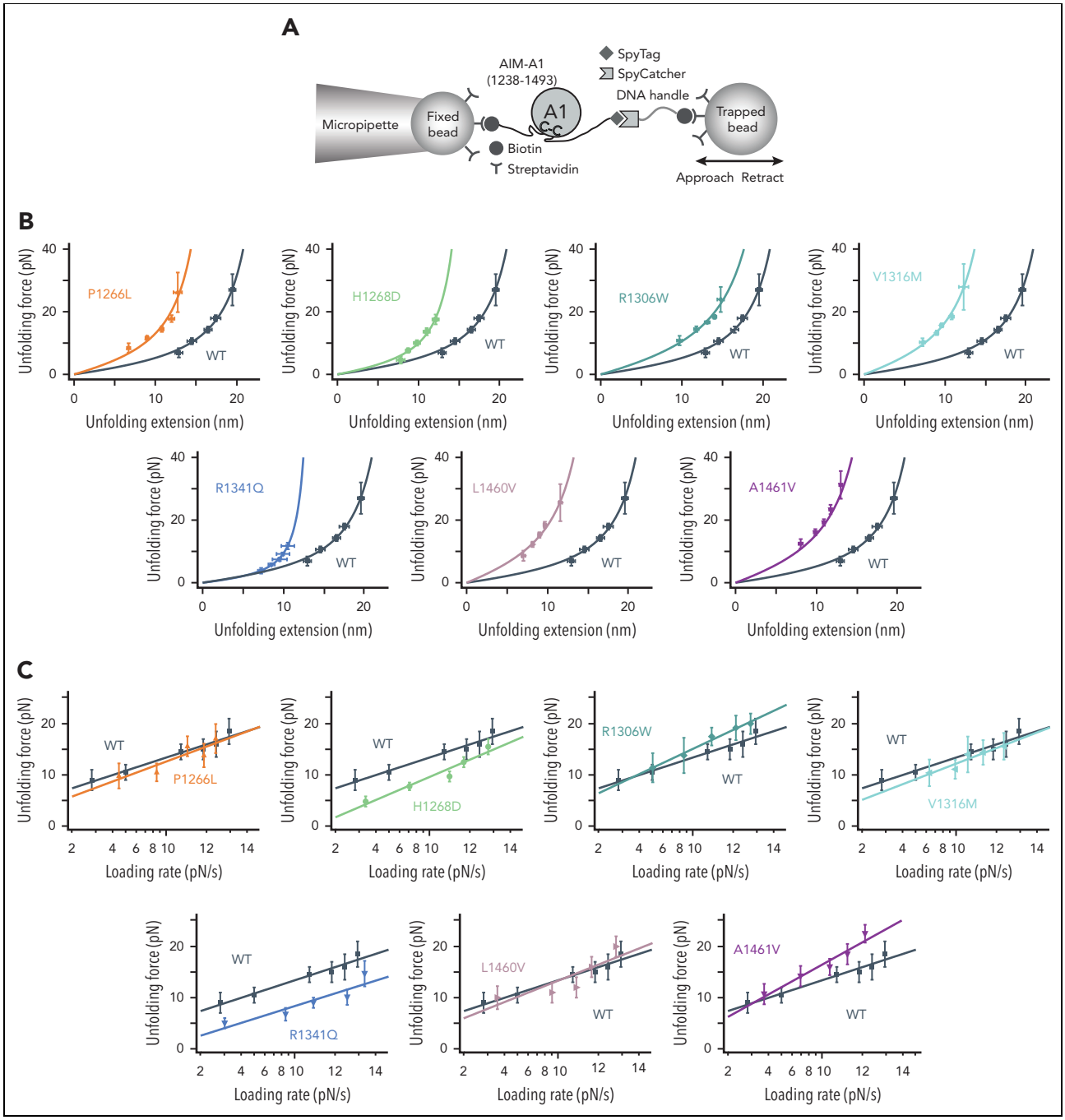

Figure 5. Single-molecule force spectroscopy data reveal the force required to unfold AIM. (A) The optical tweezers were configured with BioSpy-AIM-A1 fixed between 2 streptavidin-functionalized polystyrene beads. The biotinylated N-terminal AIM was bound directly to the fixed bead, whereas the C-terminal AIM appended with a SpyTag connected to the laser-trapped bead with a DNA handle functionalized with biotin and a SpyCatcher molecule at either end. (B) Plots of the worm-like chain model fitting results of unfolding force vs unfolding extension for each mutant compared with the WTAIM-A1. Force data are presented as mean values ± standard deviation, and extension data are presented as the peak of the Gaussian fit ± the full width at half maximum of Gaussian fit divided by the square root of counts. (C) Plots of Bell-Evans model fitting results of unfolding force vs loading rate for each AIM-A1 mutant compared with the WT AIM-A1. Unfolding force data are presented as the center of the tallest bin of the histogram ± one-half of the bin width. Numerical values of associated fittings are summarized in Table 2.

to 0.32 ± 0.07 nm from 0.60 ± 0.05 nm calculated for WT. V1316M identically reduced the persistence length to 0.32 ± 0.03 nm while simultaneously reducing the contour length to 19.6 ± 0.8 nm, suggesting that these mutations destabilize AIM-A1 coordination despite no observable direct contacts to the AIM.

Mutations P1266L, L1460V, and A1461V increased the unstressed unfolding rate (k^0_u) from the WT 0.074 ± 0.021 s^{-1} to 0.12 ± 0.08 s^{-1}, 0.13 ± 0.09 s^{-1}, and 0.12 ± 0.03 s^{-1}, respectively. These increased unstressed unfolding rates are similar to WT treated with 6G1, which we previously calculated[5] as 0.10 ± 0.05 s^{-1}, indicating that these AIM-localizing mutations, like

Table 2. Single-molecule force spectroscopy parameters associated with unfolding events of AIM-A1 variants

AIM-A1 variant	Contour length, L_C (nm)*	Persistence length, L_P (nm)*	Unstressed unfolding rate k_u^0 (s^{-1})†	Barrier position γ_u (nm)†
WT	26.6 ± 0.5	0.60 ± 0.05	0.074 ± 0.021	1.10 ± 0.10
P1266L	19.6 ± 1.9	0.41 ± 0.12	0.12 ± 0.08	0.97 ± 0.27
H1268D	17.9 ± 0.9	0.67 ± 0.11	0.29 ± 0.05	0.84 ± 0.12
R1306W	25.3 ± 2.5	0.32 ± 0.07	0.11 ± 0.02	0.76 ± 0.06
V1316M	19.6 ± 0.8	0.32 ± 0.03	0.14 ± 0.06	0.93 ± 0.18
R1341Q	15.6 ± 0.3	1.15 ± 0.08	0.27 ± 0.12	1.15 ± 0.29
L1460V	19.3 ± 1.2	0.30 ± 0.04	0.13 ± 0.09	0.89 ± 0.30
A1461V	20.7 ± 0.6	0.29 ± 0.02	0.12 ± 0.03	0.65 ± 0.09

*Contour length and persistence length are fitted worm-like chain model parameters. Uncertainties are the standard error of the fits.
†Unstressed unfolding rate and barrier position are fitted Bell-Evans model parameters. Uncertainties are the standard error of the fits.

antibody 6G1, destabilize the AIM. However, the fitted persistence lengths in these mutants are approximately half the value of WT treated with 6G1 (0.76 ± 0.19 s^{-1}), suggesting that these mutations render a different conformation to the AIM compared with the native AIM destabilized with an exogenous activator. Here, we show that all interrogated type 2B mutations disrupt AIM unfolding, although we observe no discernible link between AIM mechanics and associated bleeding complications, unlike the observed trends provided by thermodynamic and kinetic evidence.

Discussion

In this study, we show that all type 2B mutations unite by reducing the global stability of AIM-A1 protein and the mechanical force required to unfold the AIM. As a result of this compromised autoinhibition and increased plasticity of AIM-A1, all type 2B variants exhibit enhanced binding to both WT and platelet-type mutant forms of the GPIbα LBD. When investigating the conformational dynamics of AIM-A1 variants via HDX mass spectrometry, we observed that all type 2B mutants exhibited enhanced solvent accessibility in the secondary GPIbα -binding site. This enhanced solvent exposure provides a uniting structural basis separating the gain-of-function mutants from the less active WT. In addition, the AIM of all type 2B mutants released at lower forces and unfolded more rapidly compared with WT, providing additional evidence that stability of the AIM and its native contacts with disulfide-delimited A1 is pertinent for overall A1 stability and reactivity.

A long-standing question surrounding type 2B VWD is the heterogeneous clinical presentations that the mutations display, and here, we interrogate the molecular basis of this heterogeneity. The measured thermal stability for all type 2B mutants was reduced compared with WT, but the magnitude of reduction was not the same for all mutants (Figure 1). Mutation V1316M, which leads to chronic and severe thrombocytopenia,[8] resulted in the largest reduction of stability. In contrast, mutation P1266L, which is associated with normal platelet counts (supplemental Table 1), was the most stable of the represented mutants. In line with this, P1266L was the only variant to have a relative abundance of fast- and slow-dissociating molecules similar to WT (Table 1). All other variants had higher proportions of slow-dissociating molecules. The heterogeneity of the type 2B mutants was further evident in conformational dynamics of the AIM-A1 protein (Figures 3 and 4). Interestingly, HDX-reflected solvent accessibility in the β3α2 loop recapitulated trends observed in the mutants' thermal stability and the relative abundance of a high-affinity state. Since the β3α2 loop is important for ristocetin binding and GPIbα binding,[32,33] variably enhanced dynamics and solubility of this loop suggest a molecular mechanism underlying heterogeneous bleeding severity observed in patients with type 2B VWD. Overall, WT and type 2B variants exhibit heterogenous dynamic properties as a spectrum. In this spectrum, WT AIM-A1 is the most stable and bio-actively inert, with slower HDX rates in the β3α2 loop, in contrast with the phenotypically severe mutation V1316M, which showed the least stable and fastest HDX rates across most regions beyond the β3α2 loop. Mutations H1268D, R1306W, R1341Q, L1460V, and A1461V align between WT and V1316M. Mutation P1266L behaves as a hybrid between WT and these other type 2B mutants. The similarity between WT and P1266L but no other represented mutations suggest a plausible mechanism underlying accelerated depletion of platelets and HMWM of most type 2B VWD mutations. Our observations provide possible molecular signatures that may be used to evaluate other natural or synthetic mutations based on their activity (Figure 6).

This study revealed ways in which V1316M is exceptional from the other represented type 2B VWD mutants. Mutation V1316M renders AIM-A1 the least stable upon the application of heat and has more solvent accessibility across the protein as measured by HDX, with higher flexibility in the α2 and α3 helices. Therefore, in addition to having reduced mechanostability in the AIM like the other mutants, V1316M is particularly flexible in the A1 domain. An expected consequence of this flexibility is that the A1 domain may be more susceptible to conformational changes induced by tensile forces in the blood and can more effectively agglutinate platelets and clear them along with hemostatically potent multimers without requiring additional hydrodynamic forces exerted by collagen

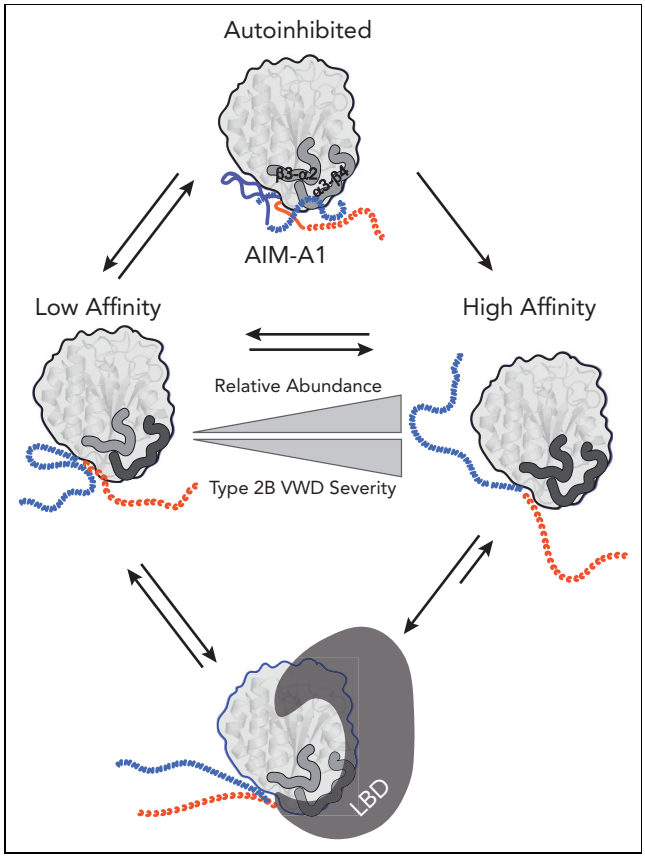

Figure 6. Proposed model illustrating type 2B VWD mutational effect on AIM-A1 thermodynamic cycling. Under normal blood flow, AIM-A1 exists in the bloodstream in an autoinhibited state because of cooperative protection from the N-terminal AIM (blue) and C-terminal AIM (orange), where both the α3β4 and β3α2 loops (light gray) have enhanced protection. Shear forces of the blood or other endogenous or exogenous factors lead to activation of the A1 domain, which equilibrates between low- and high-affinity states, in which the structure of the AIM is likely more flexible but is yet to be determined. The low-affinity A1 domain may transiently interact with GPIbα LBD as platelets roll over VWF with a higher dissociation rate constant. Based on this study, a potential molecular signature of an activated A1 domain is enhanced solvent exposure of the α3β4 loop (dark gray). The high-affinity state of the A1 domain dissociates from the LBD more slowly and can more effectively capture platelets. In this state, the A1 domain has enhanced exposure of both the α3β4 and β3α2 loops (dark gray). Severity of type 2B VWD may correlate with relative abundance of these high-affinity molecules.

immobilization. Such malleability would explain observations of small platelet aggregates in the bloodstream, loss of HMWM, and chronic thrombocytopenia in patients and mice with the V1316M mutation.[8,34,35]

Other studies have interrogated A1 thermodynamics and folding to understand the mechanics that enable VWF to stop bleeding. Studies with bacterial-derived recombinant A1 fragments showed type 2B mutations reduce the melting temperature relative to WT A1,[36-38] which stabilizes an intermediate molten globule state of the A1 domain.[39-41] Irreversibly dismantling the Cys1272-Cys1458 disulfide with a reduced and carboxyamidated (RCAM) A1 fragment or introducing an alternative disulfide yielded higher affinity to GPIbα and more effective platelet capture under arterial shear.[27,38,39,42] These observations are consistent with our data suggesting that the reduced stability observed in type 2B variants shifts the equilibrium between low- and high-affinity states, accordingly. Subsequent HDX analyses of RCAM and disulfide-bound A1 suggested that enhanced flexibility in the α2 helix and an ordered β2β3 hairpin and α3 helix describes the higher affinity conformation of the A1 domain.[42] Variable protection in the α3 helix was evident among the type 2B mutants studied here and V1316M, which showed the greatest loss of protection in this helix, supported enhanced binding to the LBD (Figure 2; supplemental Figure 2). Stipulations between the RCAM A1 and the type 2B variants studied here may not only indicate that gain-of-function mutations in AIM-A1 interfere with domain cooperativity and stability but also suggest how these mutants alter the transmission of hydrodynamic forces along the disulfide-delimited A1.

All type 2B VWD mutants investigated here have enhanced solvent accessibility in the LBD-facing α3β4 loop (Figure 4H). Regardless of HDX in other regions of the protein, all represented type 2B VWD mutants converge on this feature. Although the relative rate of HDX in this region is similar in all variants except for V1316M, there is a considerable difference in the relative deuterium uptake at all time points tested. Flexibility in this region provides a unifying mechanism underlying enhanced binding of type 2B mutants to GPIbα and is consistent with their reduced stability reported in this study and elsewhere.[36] It has previously been demonstrated in independent studies that residue Glu1376 contacts GPIbα[26] and Lys1371 forms hydrogen bonds with residues in LRR4 and LRR5 of the LBD.[27]

Although the assays performed in this study are optimal for purified proteins and not plasma VWF, which is often evaluated by clinicians and specialists that treat patients with type 2B VWD, the data presented in this study show 2 distinct regions that distinguish the gain-of-function AIM-A1 from the WT counterpart as well as a distinguishing region among type 2B VWD mutations. Curiously, all type 2B VWD mutations, including P1266L, cause bleeding in patients regardless of the extent of platelet or multimer depletion from the bloodstream. Because all tested mutations result in enhanced flexibility and loss of protection in the α3β4 loop, this region may be a key structural feature underlying reduced thermal and mechanical stability of the AIM and A1 domains. Furthermore, exposure of the β3α2 loop appears to recapitulate general bleeding severity trends at the fastest time point. Therefore, novel reagents that can target or detect the flexibility of these regions may have therapeutic or diagnostic potential.

There are 2 main forms of regulation of VWF activity. One form is through the size of the VWF multimer and its extension. Several factors, such as proteolytic cleavage of VWF multimers,[43] mutations in the C domains,[44] and partner binding that affects VWF self-association,[43,45] could affect VWF response to tensile force under flow. Although initial extension of VWF multimer under tension is not sufficient to activate A1, a follow-up extension event around the A1 domain, likely the unfolding of the AIM, exposes the A1 domain for GPIbα binding.[3,5] The other form of regulation is through allosteric conformational changes within AIM and A1. In this study, through expanded characterizations of thermo- and mechanostability and binding behavior among the type 2B variants, we

have illustrated key features within AIM and A1 that recapitulate the heterogeneous presentations at the single-domain level. Comparatively, although all 7 mutants showed reduced mechanical stability of the AIM in single-molecule force measurements, no individual mechanical parameter associated with AIM unfolding exhibited a correlation with reported bleeding severity (Figure 5). The mechanical stability of the AIM may be linked to the initial binding of A1 and the GPIbα LBD but not to A1-dependent activation of GPIb-IX and platelets. Another mechanical property, likely of the A1 domain, may govern the A1 domain's ability to undergo conformational change, sustain tension on GPIbα to induce unfolding of the mechanosensory domain, and activate platelets.[46,47] The process from the A1-LBD interaction to platelet activation entails multiple elements of protein dynamics and mechanics, including formation of the catch-bond or flex-bond between A1 and LBD.[25,48] It was reported earlier that, unlike WT, A1 protein–bearing type 2B mutations (R1306Q and R1450E) do not form a catch-bond with LBD.[48] In addition, the N-terminal AIM could stabilize the catch-bond.[49,50] The characteristics of A1 mechanics that determine the ability of VWF to activate platelets remain to be elucidated.

Acknowledgments

The authors thank Glaivy Batsuli for her helpful comments and suggestions to help tailor the manuscript to clinical audiences. The authors also thank Naifu Zhang and Sheena D'Arcy of The University of Texas at Dallas for development of HD-eXplosion, which was used for some of the hydrogen-deuterium exchange analysis presented in this study.

This work was supported, in part, by grants from the National Institutes of Health (NIH), National Heart, Lung, and Blood Institute (HL082808, HL143794, and HL153986); an infrastructure grant from Hemophilia of Georgia Center for Bleeding & Clotting Disorders of Emory; in part, by NIH (HL149357 to E.R.L., and HL154656 to N.A.A.).

Authorship

Contribution: E.R.L. and R.L. conceptualized the study; E.R.L., N.A.A., and E.T.P. performed the cloning, stable cell line generation, and protein purification; E.R.L., Y.L., N.A.A., E.T.P., and P.L. conducted the experiments; E.R.L., Y.L., P.L., X.F.Z., and R.L. analyzed the results; E.R.L. and R.L. wrote the manuscript; and E.R.L., X.F.Z., and R.L. edited the manuscript.

Conflict-of-interest disclosure: The authors declare no competing financial interests.

ORCID profiles: Y.L., 0000-0001-5937-358X; N.A.A., 0000-0002-0019-0380; P.L., 0000-0002-1206-8104; X.F.Z., 0000-0002-8778-595X; R.L., 0000-0002-5806-5080.

Correspondence: Renhao Li, Department of Pediatrics, Emory University School of Medicine, Emory University, 2015 Uppergate Drive NE, Room 440, Atlanta, GA 30322; email: renhao.li@emory.edu; and X. Frank Zhang, Department of Biomedical Engineering, University of Massachusetts Amherst, 240 Thatcher Rd, Amherst, MA 01003; email: frank.zhang@umass.edu.

Footnotes

Submitted 31 May 2022; accepted 23 December 2022; prepublished online on *Blood* First Edition 29 December 2022. https://doi.org/10.1182/blood.2022017239.

All data associated with this study are available in the main text or the supplemental Material. Data are available to academic and not-for-profit investigators upon request to the corresponding authors, Renhao Li (renhao.li@emory.edu) and X. Frank Zhang (frank.zhang@umass.edu).

The online version of this article contains a data supplement.

There is a *Blood* Commentary on this article in this issue.

The publication costs of this article were defrayed in part by page charge payment. Therefore, and solely to indicate this fact, this article is hereby marked "advertisement" in accordance with 18 USC section 1734.

REFERENCES

1. Sadler JE. Biochemistry and genetics of von Willebrand factor. *Annu Rev Biochem*. 1998; 67:395-424.
2. Springer TA. von Willebrand factor, Jedi knight of the bloodstream. *Blood*. 2014; 124(9):1412-1425.
3. Fu H, Jiang Y, Yang D, Scheiflinger F, Wong WP, Springer TA. Flow-induced elongation of von Willebrand factor precedes tension-dependent activation. *Nat Commun*. 2017;8(1):324.
4. Deng W, Wang Y, Druzak SA, et al. A discontinuous autoinhibitory module masks the A1 domain of von Willebrand factor. *J Thromb Haemost*. 2017;15(9):1867-1877.
5. Arce NA, Cao W, Brown AK, et al. Activation of von Willebrand factor via mechanical unfolding of its discontinuous autoinhibitory module. *Nat Commun*. 2021;12(1):2360.
6. Voos KM, Cao W, Arce NA, et al. Desialylation of O-glycans activates von Willebrand factor by destabilizing its autoinhibitory module. *J Thromb Haemost*. 2022;20(1):196-207.
7. Nowak AA, Canis K, Riddell A, Laffan MA, McKinnon TA. O-linked glycosylation of von Willebrand factor modulates the interaction with platelet receptor glycoprotein Ib under static and shear stress conditions. *Blood*. 2012;120(1):214-222.
8. Federici AB, Mannucci PM, Castaman G, et al. Clinical and molecular predictors of thrombocytopenia and risk of bleeding in patients with von Willebrand disease type 2B: a cohort study of 67 patients. *Blood*. 2009; 113(3):526-534.
9. Giles AR, Hoogendoorn H, Benford K. Type IIB von Willebrand's disease presenting as thrombocytopenia during pregnancy. *Br J Haematol*. 1987;67(3):349-353.
10. Makhamreh MM, Russo ML, Karl T, et al. Type 2B von Willebrand disease in pregnancy: a systematic literature review. *Semin Thromb Hemost*. 2021;47(2):201-216.
11. Weiss HJ, Sussman II. A new von Willebrand variant (type I, New York): increased ristocetin-induced platelet aggregation and plasma von Willebrand factor containing the full range of multimers. *Blood*. 1986;68(1): 149-156.
12. Woods AI, Kempfer AC, Paiva J, et al. Phenotypic parameters in genotypically selected type 2B von Willebrand disease patients: a large, single-center experience including a new novel mutation. *Semin Thromb Hemost*. 2017;43(1):92-100.
13. Holmberg L, Berntorp E, Donner M, Nilsson IM. von Willebrand's disease characterized by increased ristocetin sensitivity and the presence of all von Willebrand factor multimers in plasma. *Blood*. 1986;68(3):668-672.
14. Holmberg L, Dent JA, Schneppenheim R, Budde U, Ware J, Ruggeri ZM. von Willebrand factor mutation enhancing interaction with platelets in patients with normal multimeric structure. *J Clin Invest*. 1993;91(5):2169-2177.
15. Ginsburg D, Sadler JE. von Willebrand disease: a database of point mutations, insertions, and deletions. For the Consortium on von Willebrand Factor Mutations and Polymorphisms, and the Subcommittee on von Willebrand Factor of the Scientific and Standardization Committee of the International Society on Thrombosis and

Haemostasis. *Thromb Haemost*. 1993;69(2):177-184.

16. Rabinowitz I, Randi AM, Shindler KS, Tuley EA, Rustagi PK, Sadler JE. Type IIB mutation His-505–>Asp implicates a new segment in the control of von Willebrand factor binding to platelet glycoprotein Ib. *J Biol Chem*. 1993;268(27):20497-20501.

17. Bustamante C, Smith SB, Liphardt J, Smith D. Single-molecule studies of DNA mechanics. *Curr Opin Struct Biol*. 2000;10(3):279-285.

18. Bell GI. Models for the specific adhesion of cells to cells. *Science*. 1978;200(4342):618-627.

19. Evans E, Ritchie K. Dynamic strength of molecular adhesion bonds. *Biophys J*. 1997;72(4):1541-1555.

20. Zhang X, Halvorsen K, Zhang CZ, Wong WP, Springer TA. Mechanoenzymatic cleavage of the ultralarge vascular protein von Willebrand factor. *Science*. 2009;324(5932):1330-1334.

21. Girma JP, Takahashi Y, Yoshioka A, Diaz J, Meyer D. Ristocetin and botrocetin involve two distinct domains of von Willebrand factor for binding to platelet membrane glycoprotein Ib. *Thromb Haemost*. 1990;64(2):326-332.

22. Deng W, Voos KM, Colucci JK, et al. Delimiting the autoinhibitory module of von Willebrand factor. *J Thromb Haemost*. 2018;16(10):2097-2105.

23. Woods AI, Sanchez-Luceros A, Bermejo E, et al. Identification of p.W246L as a novel mutation in the GP1BA gene responsible for platelet-type von Willebrand disease. *Semin Thromb Hemost*. 2014;40(2):151-160.

24. Tischer A, Machha VR, Moon-Tasson L, Auton M. Platelet-type von Willebrand disease: local disorder of the platelet GPIbα β-switch drives high-affinity binding to von Willebrand factor. *J Thromb Haemost*. 2019;17(12):2022-2034.

25. Kim J, Zhang CZ, Zhang X, Springer TA. A mechanically stabilized receptor-ligand flex-bond important in the vasculature. *Nature*. 2010;466(7309):992-995.

26. Huizinga EG, Tsuji S, Romijn RA, et al. Structures of glycoprotein Iba and its complex with von Willebrand factor A1 domain. *Science*. 2002;297(5584):1176-1179.

27. Blenner MA, Dong X, Springer TA. Structural basis of regulation of von Willebrand factor binding to glycoprotein Ib. *J Biol Chem*. 2014;289(9):5565-5579.

28. Wales TE, Engen JR. Hydrogen exchange mass spectrometry for the analysis of protein dynamics. *Mass Spectrom Rev*. 2006;25(1):158-170.

29. Zheng J, Strutzenberg T, Pascal BD, Griffin PR. Protein dynamics and conformational changes explored by hydrogen/deuterium exchange mass spectrometry. *Curr Opin Struct Biol*. 2019;58:305-313.

30. Li R, Woodward C. The hydrogen exchange core and protein folding. *Protein Sci*. 1999;8(8):1571-1590.

31. Dumas JJ, Kumar R, McDonagh T, et al. Crystal structure of the wild-type von Willebrand factor A1-glycoprotein Iba complex reveals conformation differences with a complex bearing von Willebrand disease mutations. *J Biol Chem*. 2004;279(22):23327-23334.

32. Interlandi G, Yakovenko O, Tu AY, et al. Specific electrostatic interactions between charged amino acid residues regulate binding of von Willebrand factor to blood platelets. *J Biol Chem*. 2017;292(45):18608-18617.

33. Matsushita T, Meyer D, Sadler JE. Localization of von Willebrand factor-binding sites for platelet glycoprotein Ib and botrocetin by charged-to-alanine scanning mutagenesis. *J Biol Chem*. 2000;275(15):11044-11049.

34. Casari C, Berrou E, Lebret M, et al. von Willebrand factor mutation promotes thrombocytopathy by inhibiting integrin αIIbβ3. *J Clin Invest*. 2013;123(12):5071-5081.

35. Casari C, Du V, Wu YP, et al. Accelerated uptake of VWF/platelet complexes in macrophages contributes to VWD type 2B-associated thrombocytopenia. *Blood*. 2013;122(16):2893-2902.

36. Auton M, Sedlak E, Marek J, Wu T, Zhu C, Cruz MA. Changes in thermodynamic stability of von Willebrand factor differentially affect the force-dependent binding to platelet GPIbalpha. *Biophys J*. 2009;97(2):618-627.

37. Auton M, Zhu C, Cruz MA. The mechanism of VWF-mediated platelet GPIbalpha binding. *Biophys J*. 2010;99(4):1192-1201.

38. Cruz MA, Handin RI, Wise RJ. The interaction of the von Willebrand factor-A1 domain with platelet glycoprotein Ib/IX. The role of glycosylation and disulfide bonding in a monomeric recombinant A1 domain protein. *J Biol Chem*. 1993;268(28):21238-21245.

39. Tischer A, Madde P, Blancas-Mejia LM, Auton M. A molten globule intermediate of the von Willebrand factor A1 domain firmly tethers platelets under shear flow. *Proteins*. 2014;82(5):867-878.

40. Auton M, Cruz MA, Moake J. Conformational stability and domain unfolding of the Von Willebrand factor A domains. *J Mol Biol*. 2007;366(3):986-1000.

41. Tischer A, Madde P, Moon-Tasson L, Auton M. Misfolding of vWF to pathologically disordered conformations impacts the severity of von Willebrand disease. *Biophys J*. 2014;107(5):1185-1195.

42. Tischer A, Machha VR, Frontroth JP, et al. Enhanced local disorder in a clinically elusive von Willebrand factor provokes high-affinity platelet clumping. *J Mol Biol*. 2017;429(14):2161-2177.

43. Dayananda KM, Singh I, Mondal N, Neelamegham S. von Willebrand factor self-association on platelet GpIbalpha under hydrodynamic shear: effect on shear-induced platelet activation. *Blood*. 2010;116(19):3990-3998.

44. Schneppenheim R, Hellermann N, Brehm MA, et al. The von Willebrand factor Tyr2561 allele is a gain-of-function variant and a risk factor for early myocardial infarction. *Blood*. 2019;133(4):356-365.

45. Chung DW, Chen J, Ling M, et al. High-density lipoprotein modulates thrombosis by preventing von Willebrand factor self-association and subsequent platelet adhesion. *Blood*. 2016;127(5):637-645.

46. Quach ME, Dragovich MA, Chen W, et al. Fc-independent immune thrombocytopenia via mechanomolecular signaling in platelets. *Blood*. 2018;131(7):787-796.

47. Quach ME, Li R. Structure-function of platelet glycoprotein Ib-IX. *J Thromb Haemost*. 2020;18(12):3131-3141.

48. Yago T, Lou J, Wu T, et al. Platelet glycoprotein Ibalpha forms catch bonds with human WT vWF but not with type 2B von Willebrand disease vWF. *J Clin Invest*. 2008;118(9):3195-3207.

49. Zhao YC, Wang HQ, Wang Y, Lou JZ, Ju LA. The N-terminal autoinhibitory module of the A1 domain in von Willebrand factor stabilizes the mechanosensor catch bond. *RSC Chem Biol*. 2022;3(6):707-720.

50. Ju L, Dong JF, Cruz MA, Zhu C. The N-terminal flanking region of the A1 domain regulates the force-dependent binding of von Willebrand factor to platelet glycoprotein Ibα. *J Biol Chem*. 2013;288(45):32289-32301.